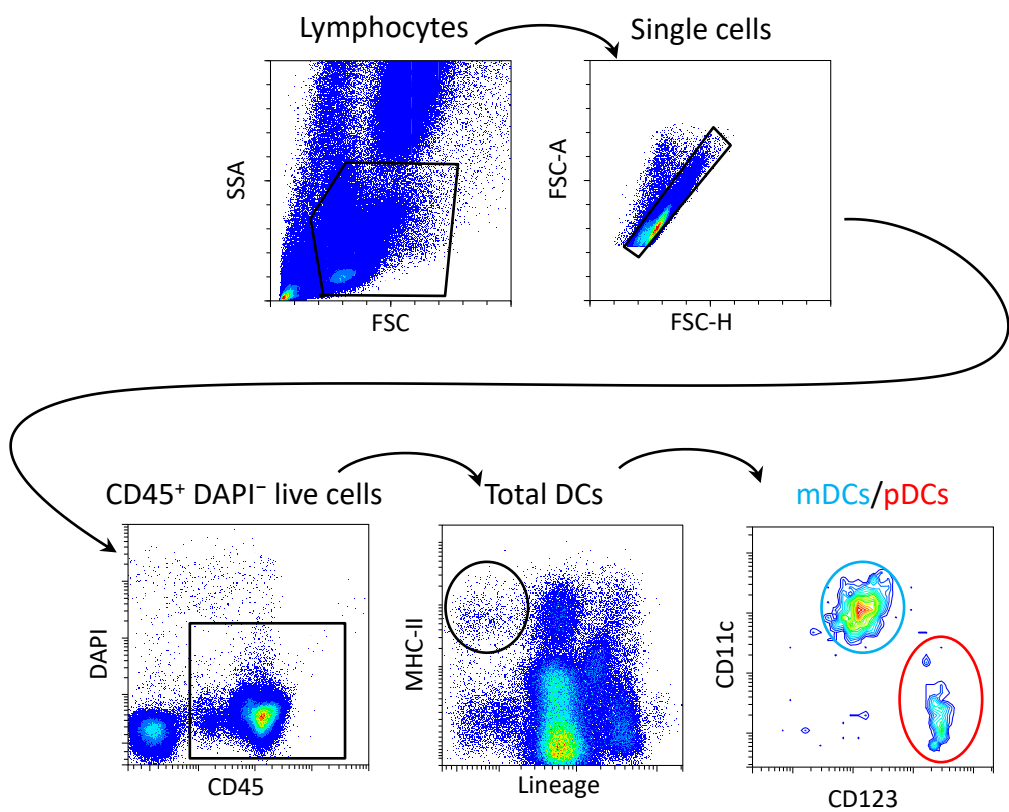The gating strategy of DC subsets

Supplementary Fig. 1. The gating strategy of human DC subsets. CD45^{+}live cells were gated from mononuclear cells, total DCs were identified as lineage cocktails (CD3, CD14, CD16, CD19, CD20, and CD56) negative and MHC-II positive, then mDCs and pDCs were detected from total DCs using CD11c and CD123 respectively. Dead cells positive for DAPI were excluded from the analysis.

IFN-α expression in different immune cells in response to CpG-ODN
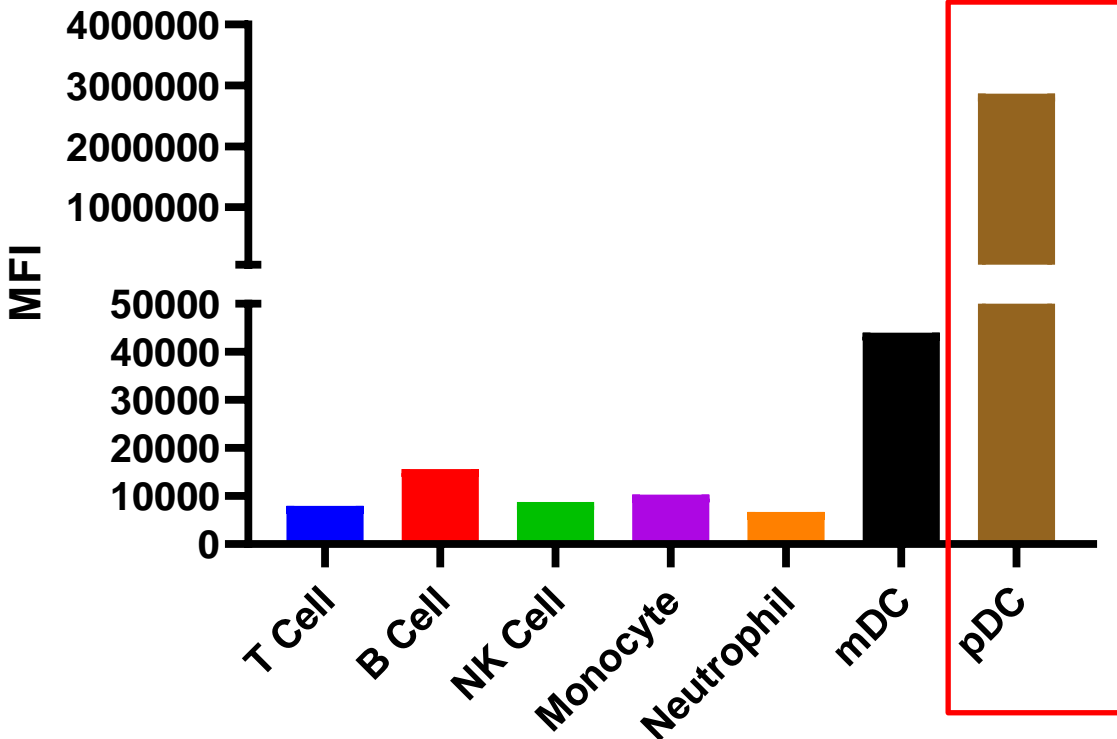
Supplementary Fig. 2. IFN-α expression in different types of immune cells in human blood after CpG-ODN stimulation. IFN-α was predominantly expressed on pDCs measured by flow cytometry. MFI: mean fluorescence intensity.
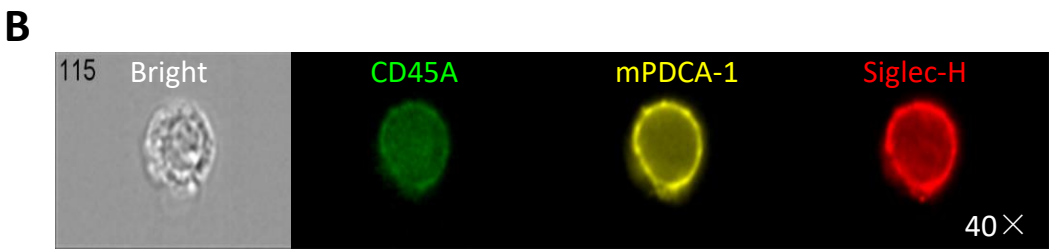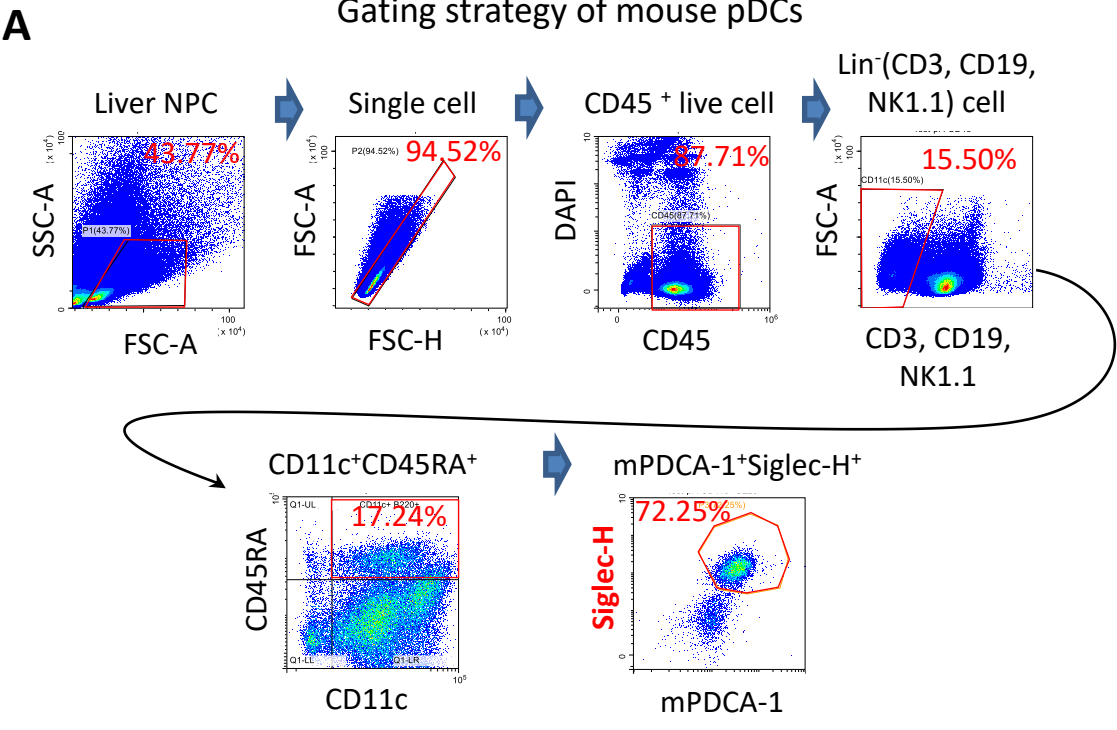
Supplementary Fig. 3

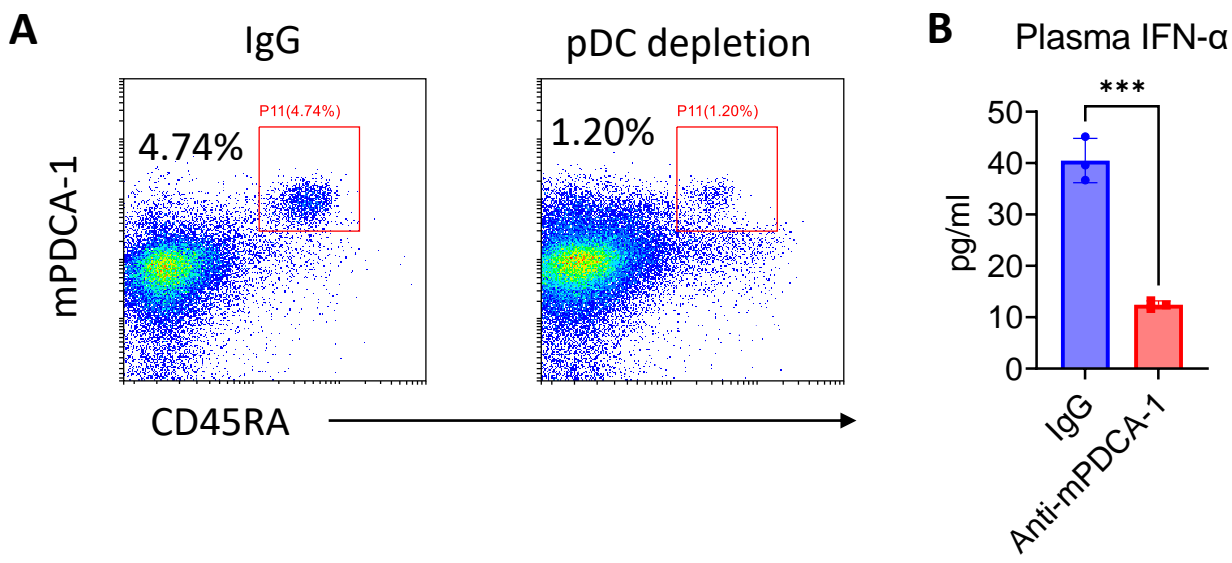The dynamics of circulating total DCs and mDCs after surgry
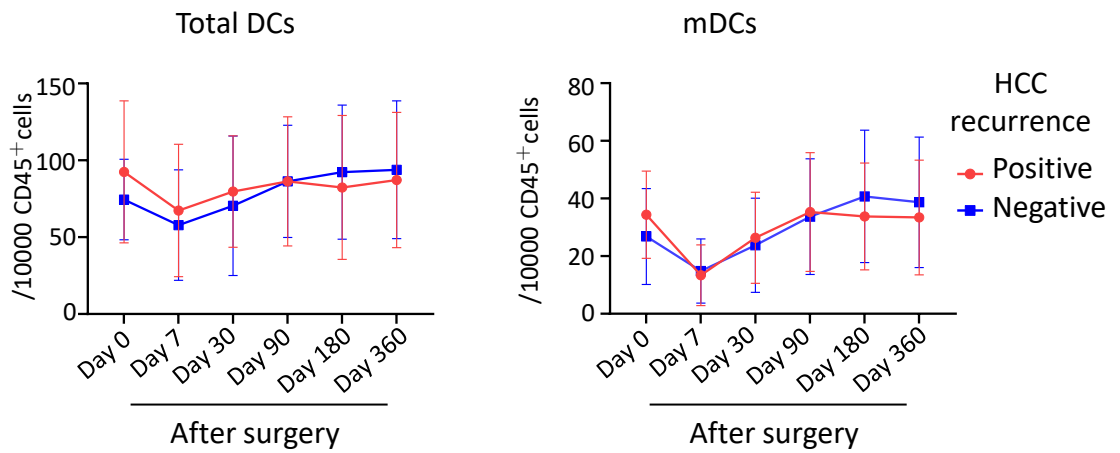
Supplementary Fig. 3. The dynamics of circulating DCs after surgery. The number of total DCs and mDCs did not show a significant difference between patients with early recurrence and patients without early recurrence.

Supplementary Fig. 4

A

Gating strategy of mouse pDCs

Liver NPC

SSC-A ($\times 10^4$)

43.77%

FSC-A ($\times 10^4$)

Single cell

FSC-A ($\times 10^4$)

P2(94.52%) 94.52%

FSC-H ($\times 10^4$)

CD45 $^+$ live cell

DAPI

87.71%

CD45(87.71%)

CD45

Lin$^-$(CD3, CD19, NK1.1) cell

FSC-A ($\times 10^4$)

CD11c(15.50%) 15.50%

CD3, CD19, NK1.1

CD11c$^+$CD45RA$^+$

CD45RA

Q1-UL   CD11c+ B220+   17.24%

Q1-LL   Q1-LR

CD11c

mPDCA-1$^+$Siglec-H$^+$

Siglec-H

72.25%

mPDCA-1

B

115 Bright   CD45A   mPDCA-1   Siglec-H   40×

Supplementary Fig. 4. Identification of mouse pDCs. A. The gating strategy of mouse pDCs. Doublets and dead cells positive for DAPI were excluded from the analysis. CD45$^+$ live cells were gated from single mononuclear cells, pDCs were identified as lineage cocktail (CD3, CD19, and NK1.1) negative and CD11c, CD45RA, mPDCA-1, and Siglec-H positive. **B.** Imaging flow cytometry showed CD45RA, mPDCA-1, and Siglec-H expression on mouse pDCs isolated from the spleen.
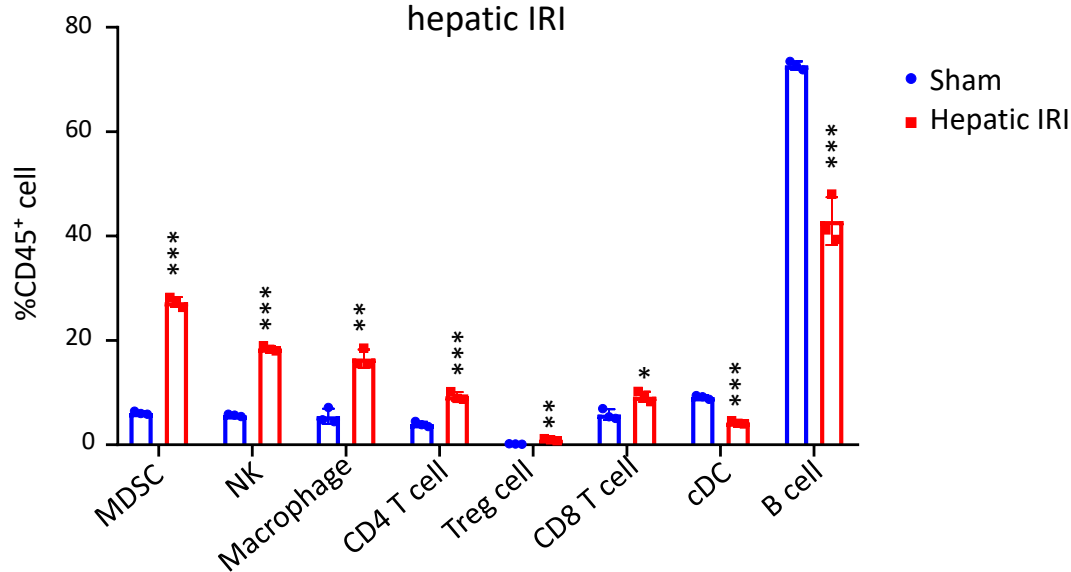
A

B

Plasma IFN-α

Supplementary Fig. 5. The effect of pDC depletion on the production of plasma IFN-α in mouse with hepatic IRI. A. Efficacy of anti-mPDCA-1 on pDC depletion. Representative dot plots show the percentage of CD45RA$^+$CD11c$^+$ pDCs among CD3$^-$CD19$^-$CD11c$^+$cells in the spleen after 3 continuous administrations with ant-mPDCA-1 antibody or IgG (250 μg/mouse/day). **B.** The concentration of plasma IFN-α in mice treated with IgG and anti-mPDCA-1 at 12 hours after hepatic IRI.

Supplementary Fig. 6

**A** Identification of CD4, CD8, Treg, B, NK, MDSC, cDC, and macrophages in mice


B
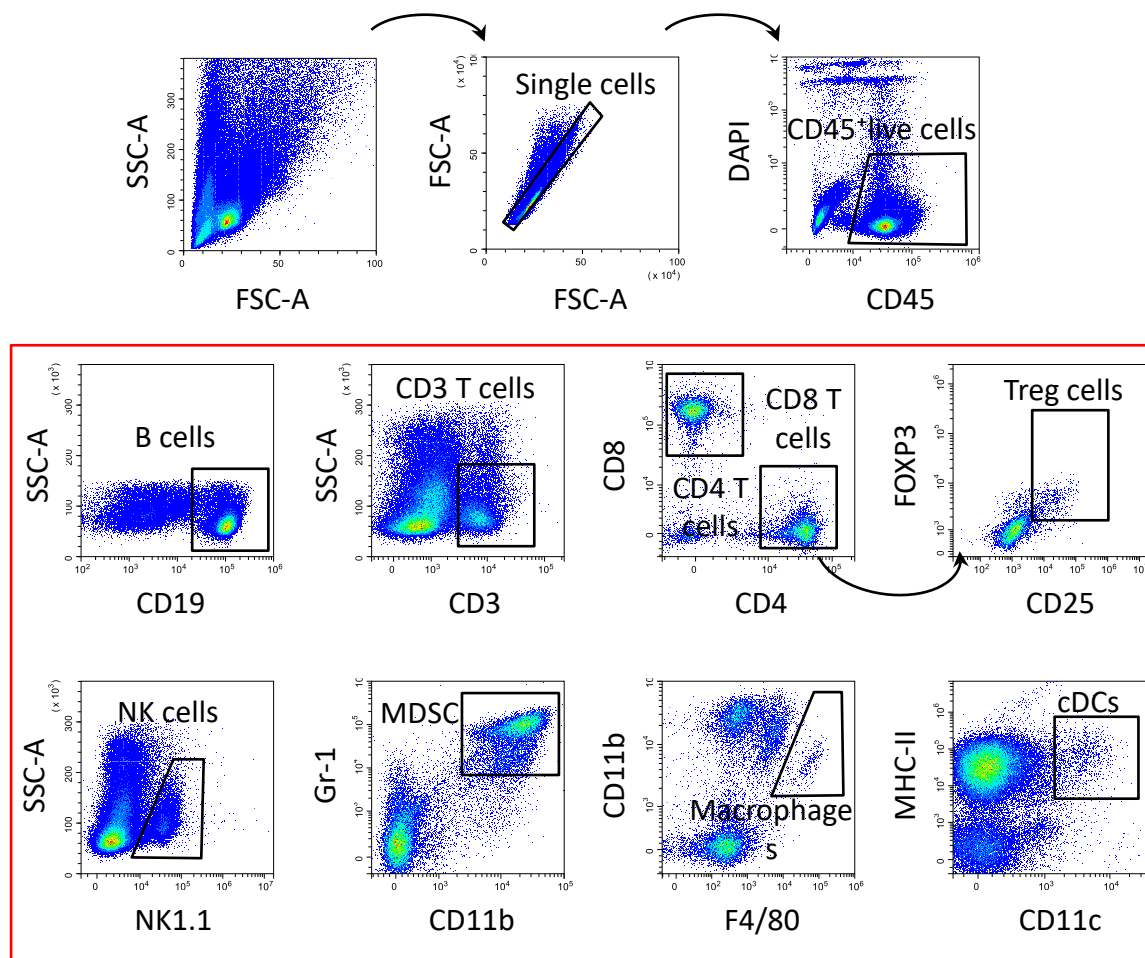
Supplementary Fig. 6. Profile of immune cell subsets in mouse livers after IRI. A. Identification of T (CD4/CD8/Treg cells), B, NK, MDSC, cDC, and macrophages in mice by flow cytometry. **B**. Number of subsets of immune cells in mouse livers at 12 hours after hepatic IRI.

Supplementary Fig. 7

CD8⁺ T cell suppression assay
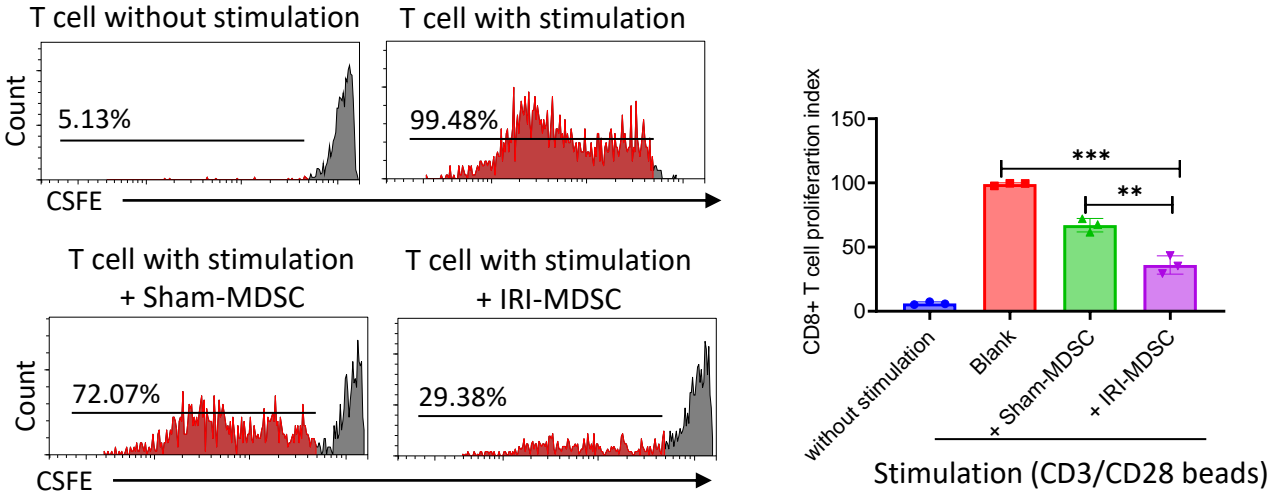
Supplementary Fig. 7. The effect of MDSCs from mice with hepatic IRI on CD8⁺ cell proliferation. MDSCs isolated from splenocytes of mice with or without hepatic IRI were co-cultured with CSFE-labeled CD8⁺T cells at a ratio of 1 : 2 for 72 hours. The proliferation rate of CD8⁺T cells was measured by flow cytometry.
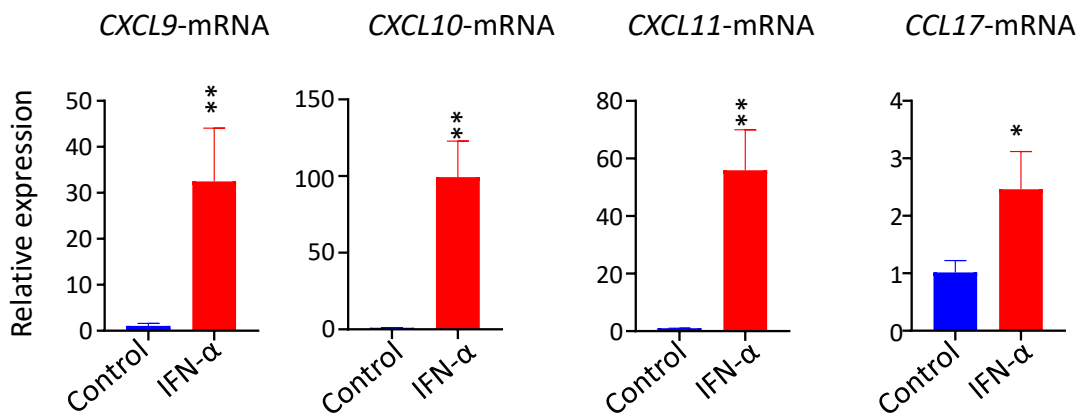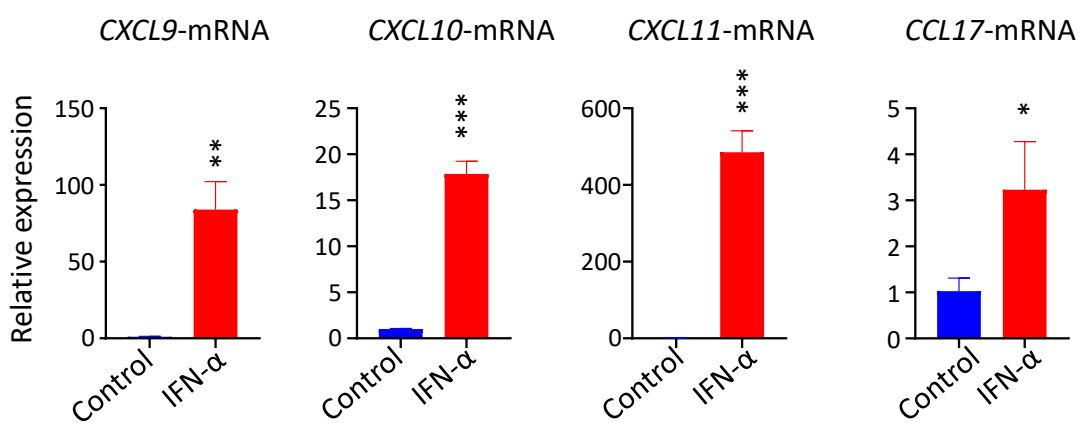
Supplementary Fig. 8
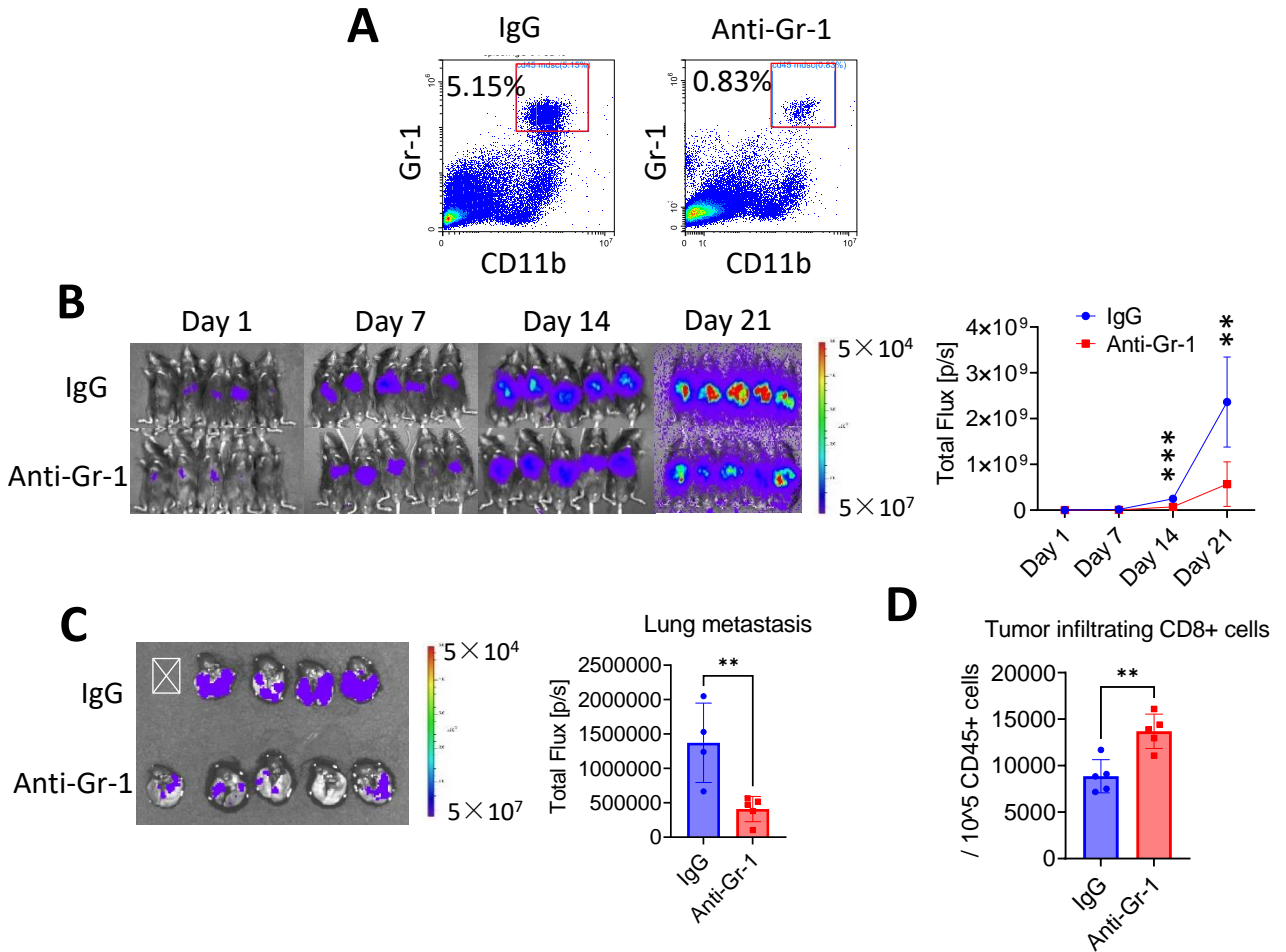
Supplementary Fig. 8. The effect of MDSC depletion on tumor progression in mice with hepatic IRI. A. Efficacy of anti-Gr-1 on MDSC depletion. Representative dot plots show the percentage of $CD11^+Gr-1^+$ MDSCs among $CD3^-CD19^-CD45^+$ cells in the spleen after ant-Gr-1 antibody or IgG treatment (200 µg/mouse/day). **B.** Tumor growth in mice treated with anti-Gr-1 or IgG measured by IVIS spectrum. **C.** Lung metastasis of tumor cells in mice treated with anti-Gr-1 or IgG 3 weeks after tumor implantation. ☒ Missing Data due to the death of the mouse. **D.** The frequency of tumor-infiltrating CD8 $^+$ in mice treated with anti-Gr-1 or IgG.
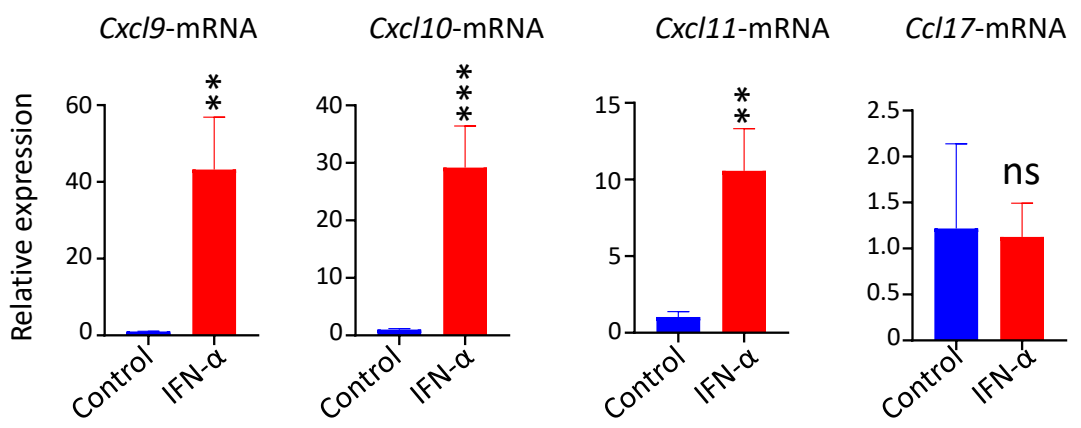
A LO2

CXCL9-mRNA   *CXCL10*-mRNA   *CXCL11*-mRNA   *CCL17*-mRNA

Huh7

CXCL9-mRNA   *CXCL10*-mRNA   *CXCL11*-mRNA   *CCL17*-mRNA

B Mouse primary hepatocytes

Cxcl9-mRNA   *Cxcl10*-mRNA   *Cxcl11*-mRNA   *Ccl17*-mRNA

Supplementary Fig. 9. Validation of gene expression upon IFN-α stimulation in human and mouse hepatocytes. A. The mRNA expression of *CXCL9, 10, 11,* and *CCL17* in human hepatocyte-like cell lines, LO2 and Huh7, treated with IFN-α. **B.** The mRNA expression of *Cxcl9, 10, 11,* and *Ccl17* in mouse primary hepatocytes treated with IFN-α.

Supplementary Fig. 10

A   Correlation between CX3CL1 and MDSCs on day 7
after surgery
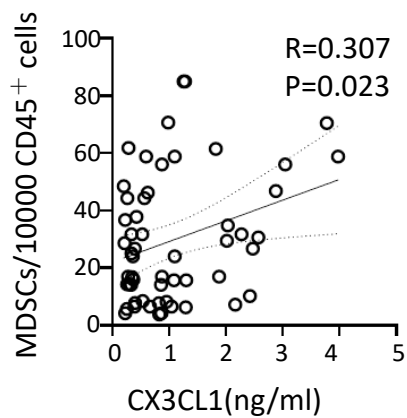
B   CX3CR1 expression on human MDSCs after surgery
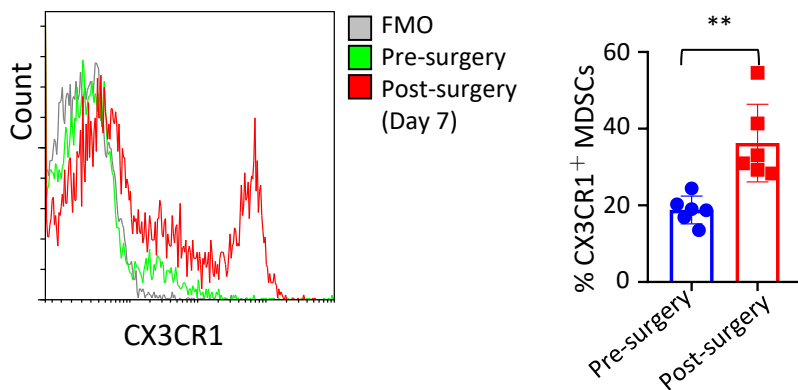
Supplementary Fig. 10. The correlation between CX3CL1 and MDSCs in HCC patients, and the expression of CX3CR1 on human MDSCs after surgery. A. The correlation between CX3CL1 and MDSCs in 55 HCC patients (Cohort 2) on day 7 after surgery. **B.** CX3CR1 expression of human MDSCs after surgery measure by flow cytometry.
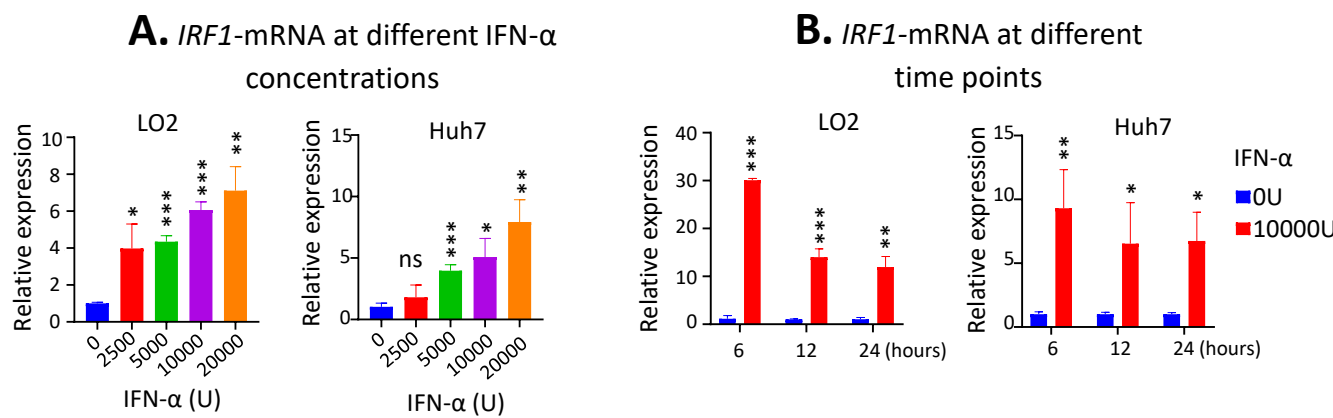
Supplementary Fig. 11
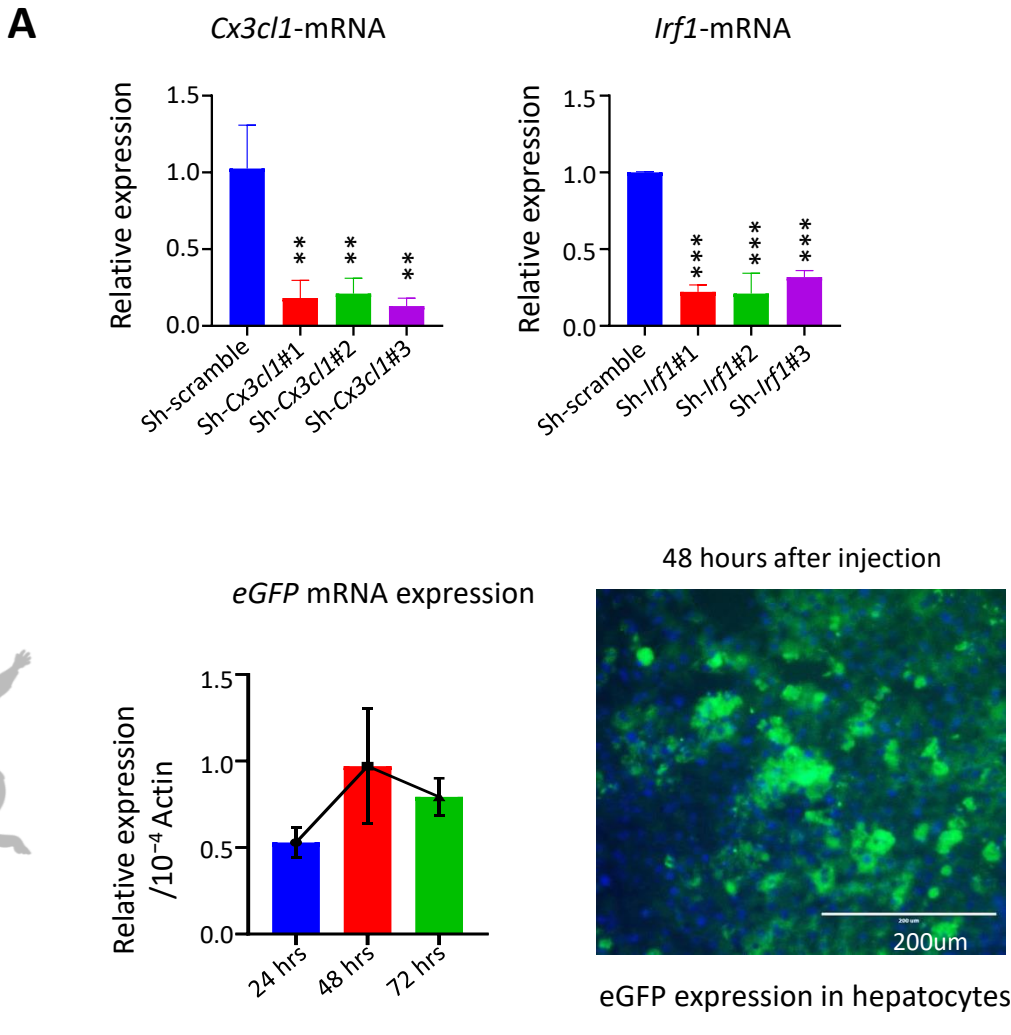

Expression of *Irf1-9* mRNA after hepatic IRI
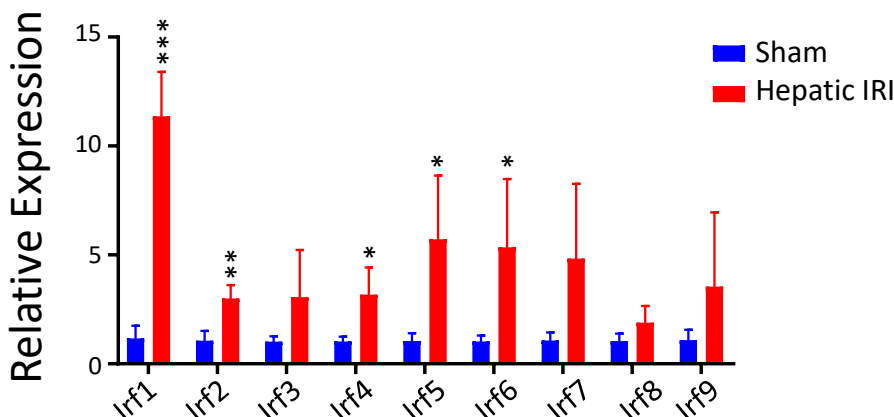
Supplementary Fig. 11. Expression of *Irf1-9* mRNA in mouse livers at 12 hours after hepatic IRI.

Supplementary Fig. 12

A. *IRF1*-mRNA at different IFN-α concentrations

B. *IRF1*-mRNA at different time points

Supplementary Fig. 12. IFN-α promoted *IRF1* mRNA expression. A. Expression of *IRF1* mRNA in LO2 and Huh7 cells in response to IFN-α at indicated concentrations. **B.** Expression of *IRF1* mRNA in response to IFN-α at different time points.

Supplementary Fig. 13

A

Cx3cl1-mRNA

Irf1-mRNA

B

eGFP mRNA expression

48 hours after injection

200um

eGFP expression in hepatocytes

Supplementary Fig. 13. Efficacy of gene transfection in vitro and in vivo. A. *In vitro* validation of *Cx3cl1* and *Irf1* mRNA downregulation using Sh-*Ifr1* and Sh-*Cx3cl1* plasmid in mouse hepatoma cells (Hepa1-6) at 48 hours after transfection. **B.** *In vivo* injection of plasmids with shRNA via hydrodynamic tail vein injection. eGFP expression was measured by qPCR and IF at 48 hours after injection.

A   **Bone marrow MDSCs in mice with or without hepatic IRI**
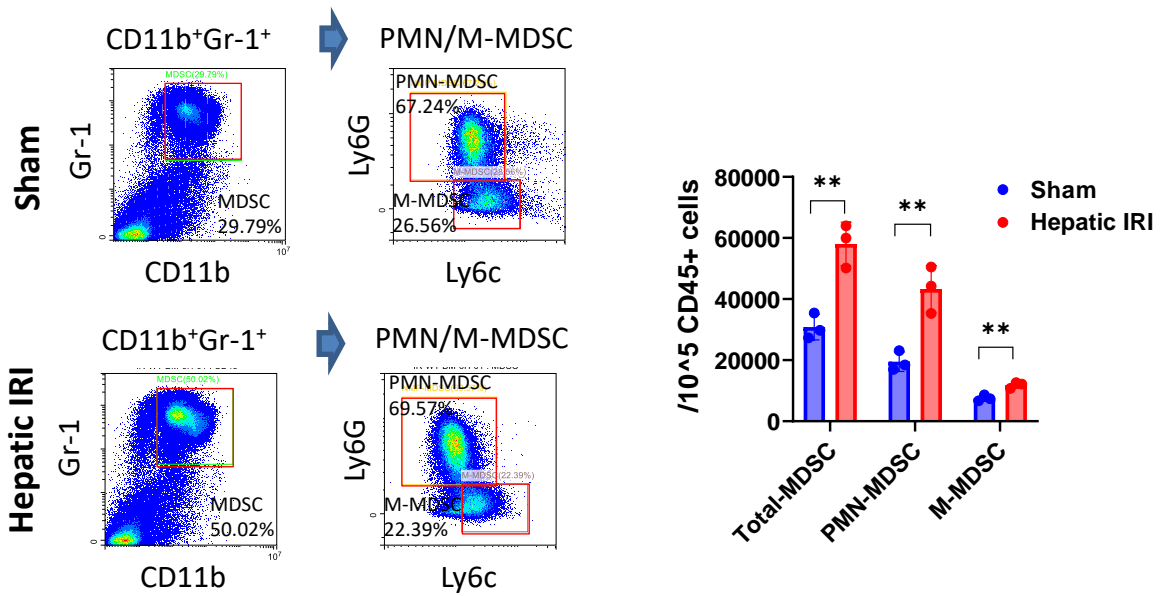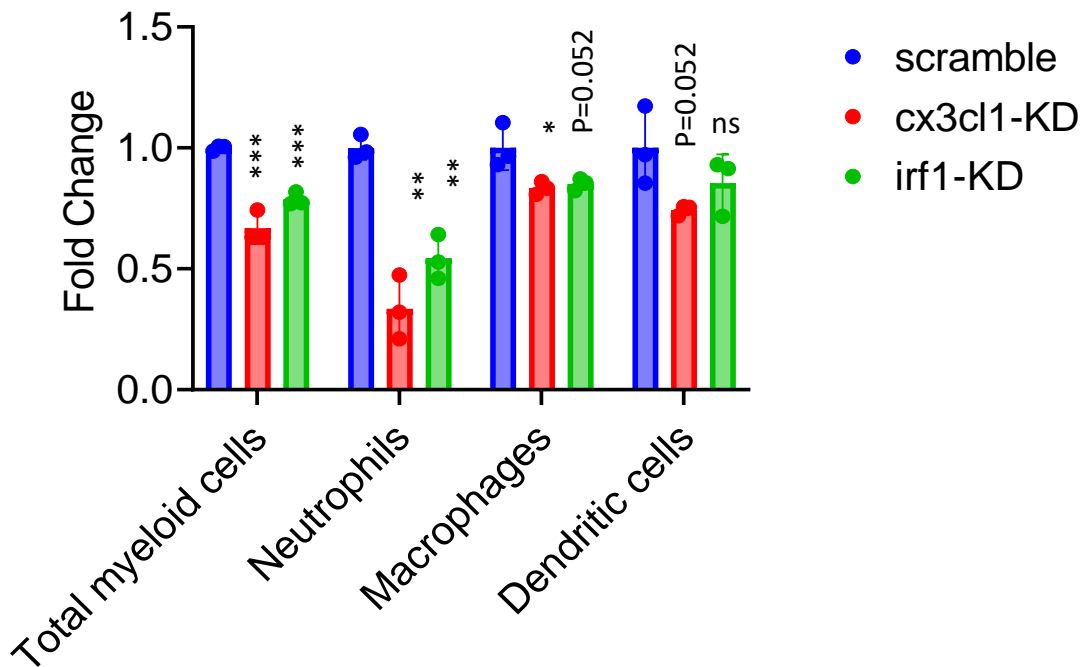

B   **The frequency of bone marrow MDSC in mice with *Cx3cl1*-KD or *Irf1*-KD following hepatic IRI**
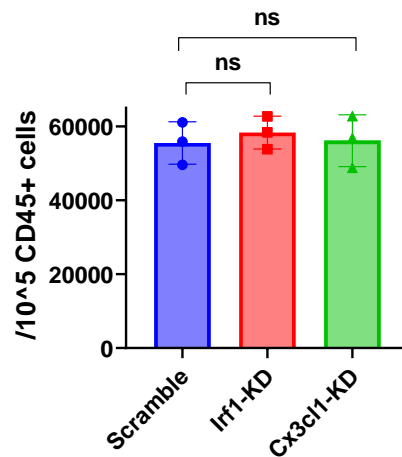

Supplementary Fig. 14. *Cx3cl1*-KD or *Irf1*-KD did not affect the expansion of bone marrow MDSCs in mice with hepatic IRI. A. The number of bone marrow MDSCs was increased 12 hours after hepatic IRI. **B.** The frequency of bone marrow MDSC in mice with *Cx3cl1*-KD or *Irf1*-KD was comparable to that in mice with scramble control following hepatic IRI.
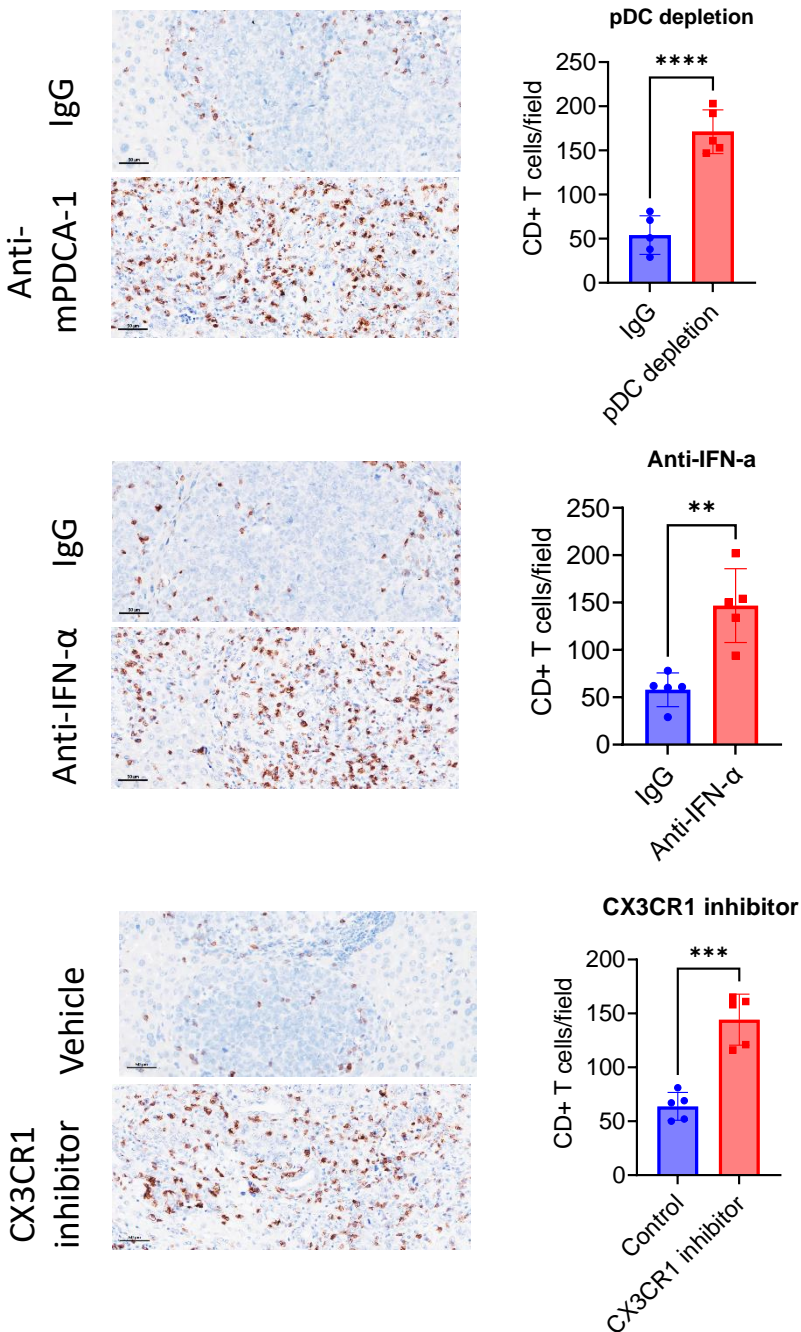
Supplementary Fig. 15. The effect of *Cx3cl1*-KD or *Irf1*-KD on mobilization of myeloid cell subsets in mice with hepatic IRI. The number of total myeloid cells, neutrophils, macrophages, and dendritic cells measured by flow cytometry in mouse livers at 12 hours after hepatic IRI.

Supplementary Fig. 16
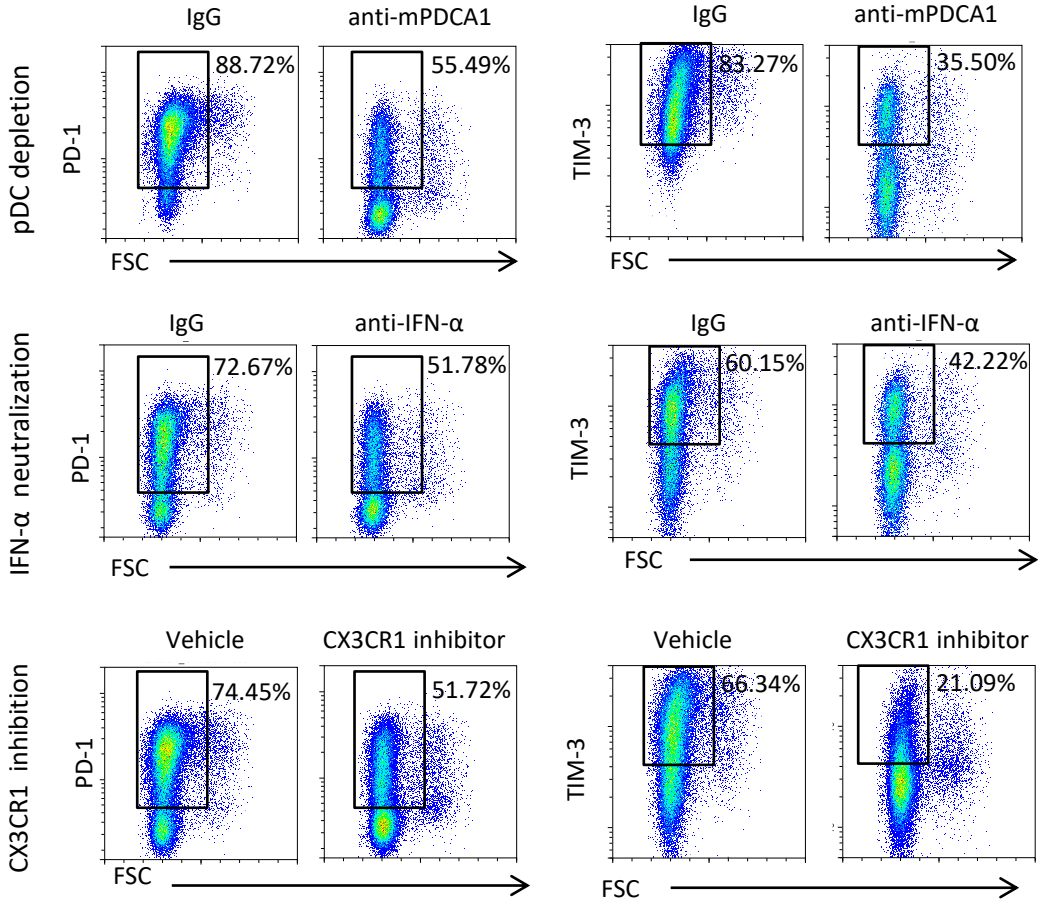
Supplementary Fig. 16. The effects of pDC depletion, IFN-α neutralization, or CX3CR1 inhibition on PD-1 and TIM-3 expression on CD8⁺ T cells.

Supplementary Fig. 17. The effects of pDC depletion, IFN-α neutralization, or CX3CR1 inhibition on CD8+ T cell infiltration. The number of CD8+ cells of each tumor was counted in 3 random high-power fields (HPF, 200 ×) under the microscope.